

Sharp depletion of radial distribution function of particles due to collision and coagulation inside turbulent flow: A systematic study

Xiaohui Meng  and Ewe-Wei Saw *

School of Atmospheric Sciences and Guangdong Province Key Laboratory for Climate Change and Natural Disaster Studies, Sun Yat-Sen University, Zhuhai 519000, China



(Received 4 January 2023; accepted 28 June 2023; published 18 August 2023)

The clustering (preferential concentration) and collision of particles in turbulent flows is a significant process in nature, such as in the precipitation process of atmospheric clouds. We perform direct numerical simulation (DNS) to study the clustering of small, heavy, monodisperse particles subject to collision-coagulation in turbulent flow [i.e., colliding particles always coagulate (coalesce) into larger ones]. The simulations do not include gravitational effects and hydrodynamic interactions among particles. We find that collision-coagulation causes the radial distribution function (RDF) of the particles to decrease strongly at particle separation distances r close to the particle diameter d . However, we observe that the RDF does not decrease indefinitely but approaches a finite value in the limit of $r \rightarrow d$. We study how the properties of this “depletion zone” relates to the particle Stokes number (St), particle diameter, and the Reynolds number of the turbulent flow. A collision-induced modulation factor γ_c is defined to represent the degree of RDF depletion due to collision-coagulation. In the region where $\gamma_c(r)$ is a quasi-power-law, we find that the effective power-law exponent \tilde{c}_1 depends only weakly on St in the regime of $St \ll 1$, but increases significantly for larger St and peaks at around $St \approx 0.7$. The same qualitative trend is also observed for the limiting values of γ_c at $r \rightarrow d$. We find that the overall trend of \tilde{c}_1 with respect to St is qualitatively similar to that of the classical power-law exponent c_1 appearing in the RDF of noncolliding particles, except that \tilde{c}_1 is barely changed at small St and the magnitude of the trend is much weaker. A complementary investigation on the Stokes number trend of the full RDF in the depletion zone is performed. The slope of the RDF appears to be constant for $St \ll 1$ but changes as St becomes large. The location of the RDF’s peak is found to be St-dependent. We found that the depletion zone is insensitive to the flow Reynolds number and that γ_c of different Re_λ overlap. As the particle diameter d changes, the reduction of the RDF occurs on scales that shift accordingly, and always starting at around $2.4d-3d$. We also find that the shape of $\gamma_c(r)$ is independent of changes in d .

DOI: [10.1103/PhysRevFluids.8.084304](https://doi.org/10.1103/PhysRevFluids.8.084304)

I. INTRODUCTION

The fluctuation of particle concentration has a profound effect on interparticle collisions. This effect has a pivotal role in both natural sciences and industrial engineering. For example, the collision-coagulation process for small droplets (particles) determines their spatial and temporal size distribution. These microscale properties have significant influences on the formation of precipitation [1]. Small-scale turbulence in clouds makes an important contribution to the collision

*Also at Ministry of Education Key Laboratory of Tropical Atmosphere-Ocean System, Zhuhai 519000, China; corresponding author: ewsaw3@gmail.com

and coagulation of droplets [1,2]. Another example is the formation of planetesimals. The collision of dust in protoplanetary disks sets the stage for planet formation. Research shows that the turbulent motion concentrates dust in the dissipation scale, increasing the collision rate of dust particles [3–5]. In industry, the clustering and collision of particles will impact on the effect of combustion of pulverized fuel flames [6].

The preferential concentration of inertial particle has become a prevalent research topic since the end of the 20th Century. Squires and Eaton [7] found that the inertial particles preferentially concentrate in regions of low vorticity and high strain rate. The degree of particle clustering can be characterized by the radial distribution function (RDF), which is defined as the ratio of the probability of finding a particle pair at a distance r normalized by the probability of the same event for random particle distribution. Reade and Collins [8] found that the clustering of small particles occurs on a scale that is much smaller than the Kolmogorov length scale, and that the RDF of particles follows a negative power law with the interparticle separation distance r . Chun *et al.* [9] developed a drift-diffusion theory to predict the RDF in turbulent flows for particles in the limit of small particle Stokes number. Their results show that the RDF of particle is proportional to $c_0(r/\eta)^{-c_1}$, where η is the Kolmogorov length scale. They also find that the exponent c_1 is proportional to St^2 . The Stokes number (St) is an important measure of particle inertia, and is defined as the ratio of the particle relaxation time τ_p and the Kolmogorov timescale τ_η . The dissipation-scale clustering of particles becomes stronger as the Stokes number increase and the RDF reaches a peak near the Stokes number of order unit [10]. This relationship between the RDF and the Stokes number is corroborated by both numerical and experimental studies [11,12].

The calculation of collision kernel is still an open question. Saffman and Turner [13] estimate collision rates of small water droplet (e.g., inertialess particles) in turbulent rain clouds. Gustavsson *et al.* [14] give an extension of the Saffman-Turner formula and derive exact expressions for the steady-state collision rate for inertialess particles suspended in rapidly fluctuating random flows. The preferential concentration of particles is expected to enhance particle collision. In the work of Sundaram and Collins [15], the RDF was first introduced into the formula of collision kernel using the spherical formulation [16]: $K = 2\pi d^2 \langle w_r \rangle g(d)$, where d is the particle diameter, $g(d)$ is the particle RDF at contact, w_r is the radial component of the two-particle relative velocity. The works on the RDF of particles mentioned thus far had used the ghost particle assumption and ignored the effect of collision and coagulation among particles. Saw and Meng [17] found that the RDF drops sharply at r close to d in the presence of collision-coagulation and provided a theoretical account of this finding and the nontrivial relationship among RDF, collision rate and relative particle motions. These findings are interesting because they highlight the importance of accounting for actual particle collisions, and also question the formula of collision kernel mentioned above.

In this paper, we use direct numerical simulation (DNS) to study the monodispersed RDF of the inertial, colliding, particles. DNS, which solves the Navier-Stokes equation fully in the spatial and temporal scales without using any turbulence modeling, is an efficient numerical tool to study the particle-laden turbulent flow. The RDF of particles considering the effect of the collision-coagulation is investigated. The influence of the particle and turbulent parameters on the decrease of RDF is also studied in this paper. The paper is organized as follows: Sec. II provides a summary of the simulation methods and the relevant turbulent and particle parameters. The statistical results and discussion are presented in Secs. III and IV, respectively. Finally, the results of the influence of the turbulent and particle parameters on the RDF are summarized in Sec. V.

II. SIMULATION METHOD

We performed the direct numerical simulation (DNS) of the particle-laden turbulent flow. The incompressible Navier-Stokes equations are shown below.

$$\frac{\partial \vec{u}}{\partial t} + \vec{u} \cdot \nabla \vec{u} = -\frac{1}{\rho} \nabla p + \nu \nabla^2 \vec{u} + \vec{f}(\vec{x}, t), \quad (1)$$

$$\nabla \cdot \vec{u} = 0. \quad (2)$$

TABLE I. The DNS parameters and time-averaged statistics. N is the simulation grid size, ν is the kinematic viscosity of turbulence, ϵ is the dissipation rate of turbulent flow, u' is the root-mean-square velocity of turbulent flow, λ is the Taylor length scale, η and τ_η are the Kolmogorov length and timescale, L and T_L are the integral length and timescale, Re_λ is the Taylor scaled Reynolds number.

	N	ν	ϵ	u'	λ	η	τ_η	L	T_L	Re_λ
Flow 1	256	0.001	0.0326	0.3519	0.2386	0.0132	0.1750	0.5073	1.4416	84
Flow 2	256	0.001	0.1013	0.5684	0.2187	0.0100	0.0993	0.6151	1.0822	124
Flow 3	512	0.001	0.9472	1.226	0.1544	0.0057	0.0325	0.7398	0.6034	189

The N-S equations are solved numerically on N^3 grids cube using a pseudospectral method on the periodic domain, the length of which is 2π . The turbulent velocity \vec{u} is transformed from physical space to wave-number space. The aliasing error arising from the convection part of the N-S equation, is removed by the 2/3-method [18]. $\vec{f}(\vec{x}, t)$ in the N-S equation is an external forcing conducted at low wave number to maintain statistically stationary [19]. To study the influence of the (Taylor scaled) Reynolds number on the RDF, simulations with different Re_λ are conducted: $\text{Re}_\lambda = 84, 124,$ and 189 , the detailed turbulent parameters are given in Table I. For different Reynolds numbers, the grid size is $N = 256$ (for $\text{Re}_\lambda = 84$ and 124) and 512 (for $\text{Re}_\lambda = 189$). The small-scale resolution can be characterized by $k_{\max}\eta = 1.59, 1.21,$ and 1.38 , respectively, where $k_{\max} = N\sqrt{2}/3$ is the maximum resolved wave-number magnitude. The 2-order Runge-Kutta method is used to perform time advance in the N-S equation. The Courant number $C = 0.0248, 0.0401,$ and 0.0865 . The energy spectra for different flow are shown in the Appendix A. A higher resolution simulation is conducted to study the possible effects of the sub-Kolmogorov intermittency on our results, using $N = 1024$ at $\text{Re}_\lambda = 124$. This is detailed in Appendix B.

The particles we consider are small (the diameter of the particle d is smaller than the Kolmogorov length scale η) and heavy (the density of the particle is greater than that of the flow). Since only basic questions are of interest in this paper, the gravitational effect and the interparticle hydrodynamic interactions are not included in the DNS. The limit of small (pointlike) particles is assumed, the spherical size of the particle is only considered in the collision processes. And only one-way coupling to the turbulent flow is considered. Under these circumstances, the particles are only subjected to viscous Stokes drag force, and the following motion equation of the particles [20]:

$$\frac{d\vec{v}}{dt} = \frac{\vec{u}(\vec{x}, t) - \vec{v}}{\tau_p}, \quad (3)$$

where \vec{v} is the particle velocity, and $\vec{u}(\vec{x}, t)$ is the fluid velocity at the particle position. τ_p is the particle inertial response time, defined $\tau_p = \frac{1}{18} \frac{\rho_p d^2}{\rho \nu}$, where ρ_p and ρ are the particle and fluid densities, respectively, d is the particle diameter, and ν is the kinematic viscosity of the turbulent flow. The linear interpolation method is used to interpolate the velocity of the flow in the particle position, and the 2-order Runge-Kutta method with “exponential integrators” is used for the time advance [21].

Spherical and monodisperse particles are randomly introduced into the simulation. Particles collide when their volumes overlap and a new particle is formed, conserving volume and momentum. New particles are injected at random locations in the system at fixed time intervals so that the particle system reaches a steady state after a transient period and the average number of particles in steady state is in a range of $5.4\text{--}9.8 \times 10^6$ for different St cases.

We want to compare the difference between the RDF in the case of collision-coagulation and the case using noncolliding ghost particles. Hence, we calculate the RDF of monodisperse particles:

$$g(r) = \frac{\psi(r)/N}{(N-1)\delta V_r/V}, \quad (4)$$

TABLE II. Characteristics of the runs discussed here. Re_λ is the Taylor microscale Reynolds number of the fluid. d is the particle diameter, $d_* = 9.49 \times 10^{-4}$. St is the particle Stokes number. When St is varied, to keep the particle diameter constant, the particle mass density is changed.

Run	Re_λ	d	St
1	124	d_*	0.01
2	124	d_*	0.05
3	124	d_*	0.1
4	124	d_*	0.2
5	124	d_*	0.5
6	124	d_*	0.7
7	124	d_*	1.0
8	124	d_*	2.0
9	124	$\frac{1}{3}d_*$	0.1
10	124	$3d_*$	0.1
11	84	d_*	0.1
12	189	d_*	0.1

where $\psi(r)$ is the sum over the number of particles found at distance r from each primary particle, $\delta V_r/V$ is the ratio of an infinitesimal volume at distance r to the total sample volume. To study the influence of particle parameters on the RDF, particles with different Stokes numbers from 0.01 to 2.0 are introduced in each simulation. Particle size is another important parameter related to particle collision. Three different sizes of particles are introduced in each simulation: $d = \frac{1}{3}d_*$, $d = d_*$, and $d = 3d_*$, where $d_* = 9.49 \times 10^{-4}$. The details of the simulations are listed in Table II. The statistics are calculated for monodispersed particles.

III. RESULTS

A. Stokes number dependence

The statistics from Run 1 to Run 8 in Table II are used to study the influence of the Stokes number on RDF. The RDFs for particles with different Stokes numbers are shown in Fig. 1. What is striking in this figure is the strong decrease of the RDF when the particle separation distance r is close to the particle diameter d . Figure 1 also shows that there is an increase in the slope and the magnitude of the RDF at the scales $r/\eta \sim 1 - 10$ when St is increased from 0.01 to 0.7. Note that the slope of the RDF is smaller for $St = 1.0$ than that for $St = 0.7$, although its values are larger everywhere. Beyond $St = 1.0$, both the slope and the magnitude decrease from $St = 1.0$ to $St = 2.0$. At larger scales ($r/\eta \sim 10$), the RDF curves flatten and converge to 1. To elucidate the trend of the RDF when the separation distance r is close to the particle diameter d , the RDFs are plotted as a function of $r - d$ in Fig. 2. The most interesting aspect of this graph is that the relationship between RDF and $r - d$ shows a quasi-power-law trend in the range of $4 \times 10^{-5} \lesssim r - d \lesssim 3 \times 10^{-4}$. As r continues to decrease toward the particle diameter, the slope of the RDF gradually becomes smaller and tentatively approaches zero, i.e., the RDF tentatively approaches a plateau.

The same reduction in RDFs near particle contact ($r = d$) has already been observed by Saw and Meng [17], including some evidence that suggests a plateau regime in the limit of $r \rightarrow d$. However, the resolution (in r) in that study was too limited for a strong conclusion in this respect, and a tentative plateau was only successfully shown for one Stokes number value. One goal of the present study is to remedy this limitation, and this is partially addressed by Fig. 2, while results with significantly higher resolution shall be presented in the sequel.

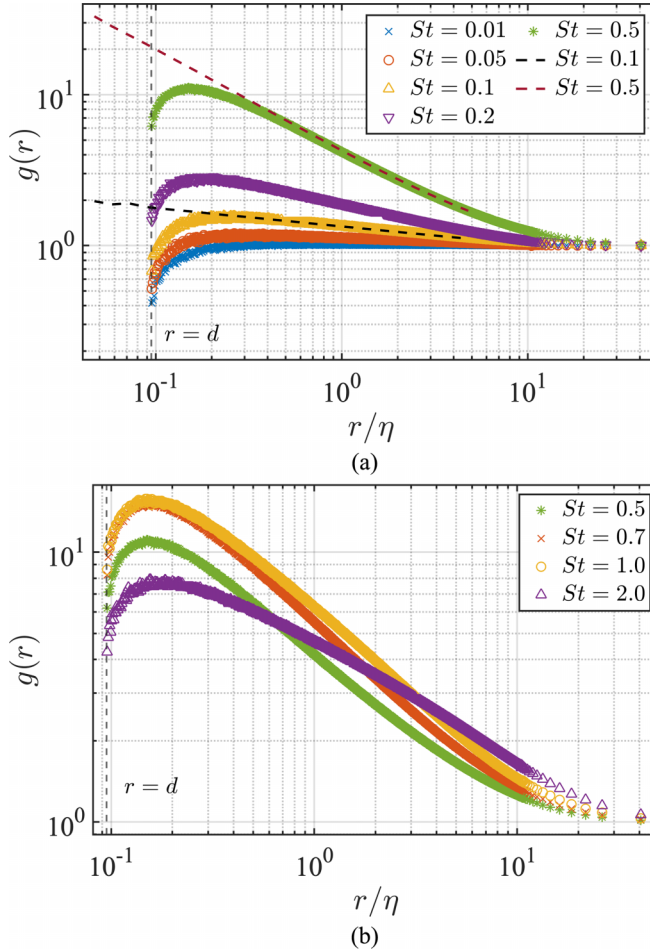


FIG. 1. The RDFs versus r/η for particles with different Stokes number. The diameter of particle is $d = 9.49 \times 10^{-4}$ and the Taylor scaled Reynolds number is $Re_\lambda = 124$. The dashed lines are RDFs for noncolliding monodisperse particles, $St = 0.1$ and $St = 0.5$, respectively. In comparison, the RDFs of the cases with coalescing particles drops significantly when r is close to d .

At this point, it is appropriate to provide some explanation and interpretation of the observations thus far. Saw and Meng [17] have presented a detailed theoretical treatment of the problem and shown that the form of RDF observed here could be theoretically predicted starting from a few physically motivated (and intuitive) assumptions on the relative motions of the particles. Here, we attempt to provide an intuitive account of the basic ideas behind the theory (more rigorous details can be found in Ref. [17]) that could explain the reduction of RDF seen here. As illustrated in Fig. 3, P and S represent two particles of identical diameter. Using particle P as a reference particle, \vec{r} denotes the position of particle S relative to P. When r approaches the particle diameter d , which is smaller than the Kolmogorov length scale, it can be assumed that the trajectory of the particle at this scale is almost rectilinear, since the radius of curvature of all particle trajectories should be no smaller than η (η being the smallest scales of turbulent undulations). Let \vec{v} be the relative velocity of S in the frame of P. The two particles will collide and coagulate when r is less than or equal to the sum of their radii (i.e., the diameter d of the particle). Consequently, the angle between \vec{v} and \vec{r} of any realizable trajectory cannot be less than θ_m , where $\sin(\theta_m) = d/r$ (see Fig. 3), since otherwise a coalescence event would have occurred and the pair would have vanished from the scope of the

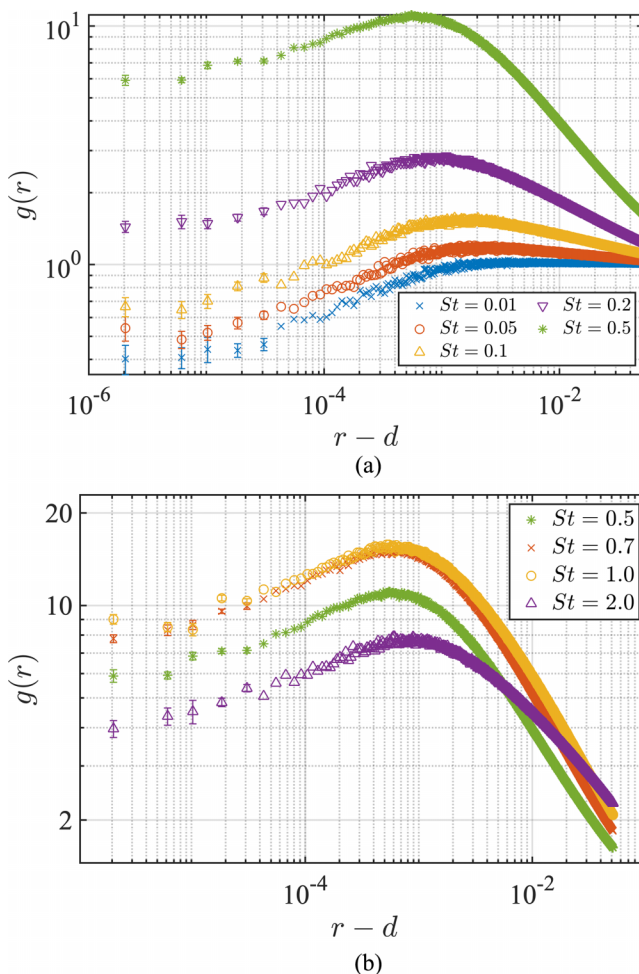


FIG. 2. The RDFs versus $r - d$ for particles with different Stokes number, $d = 9.49 \times 10^{-4}$ is the particle's diameter. The Taylor-scaled Reynolds number is $Re_\lambda = 124$ in this case. Error bars represent one standard error. The RDF follows a quasi-power-law with $r - d$ in the range $0.04d \lesssim r - d \lesssim 0.3d$ and the slope of RDF decreases to zero gradually as r continues to decrease.

monodisperse analysis (e.g., the computation of the RDF of single sized particles). This results in a deficit of particle pairs at these distances relative to the ghost particle case.

However, at significantly larger scales in r , the assumption of nearly rectilinear trajectories breaks down, thus particles could have arbitrary velocity directions without implying a collisional history with neighbors (this was implied but not explicitly stated in Ref. [17]). RDFs recover their ghost particle form at these scales.

Figure 4 shows the trend of RDF as r decrease toward d with significantly higher resolution, using the cases of $St = 0.1$, $St = 0.2$, and $St = 0.5$ as examples. It provides stronger evidence for the conjecture that when r is close to d (e.g., for $r - d$ is less than 4×10^{-6}), the RDF no longer decreases but approach a fixed value. The limiting value of the RDF at particle contact ($r = d$) is proportional to the particle collision rate [15], thus a finite collision rate in our simulations should imply that the value of RDF should be equal to a, fixed, noninfinitesimal value. The results shown above are consistent with this analysis.

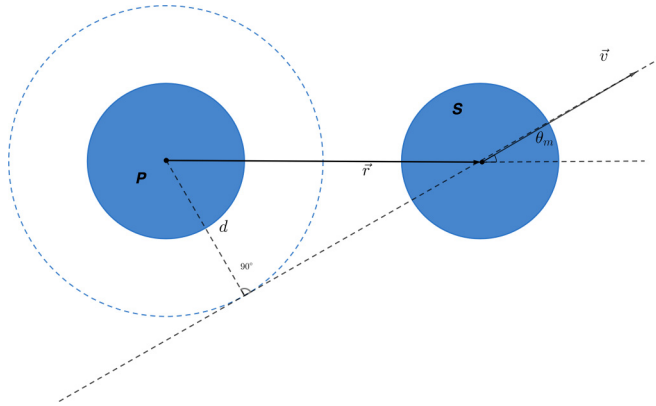


FIG. 3. Schematic illustrating the ideas behind the theory in Ref. [17] that explain the reduction of RDF in the regime of $r \approx d$. P and S are two particles with the same diameter and St . The relative position of the S particle to the P particle is represented by \bar{r} , while \vec{v} represents the relative velocity of S to P. More details in the main text.

We shall call the region where the RDF decreases, as seen in Fig. 4, the “depletion zone.” Subsequent discussions will mainly focus on this region.

It is important to note that we have investigated the possible influence of unresolved sub-Kolmogorov intermittency on the accuracy of our RDFs results and the outcomes is described in Appendix B section. Our findings suggest that sub-Kolmogorov scale intermittency may slightly modify the clustering exponent of the RDF, resulting in an upward shift of all small-scale features of the RDF by the same order of magnitude (see the Discussion and Appendix B for details). As a consequence, the value of the RDF may be underestimated by a few percent. However, the effect on the shape of the RDF curve is minimal and does not significantly impact our main conclusions to be presented in sequel.

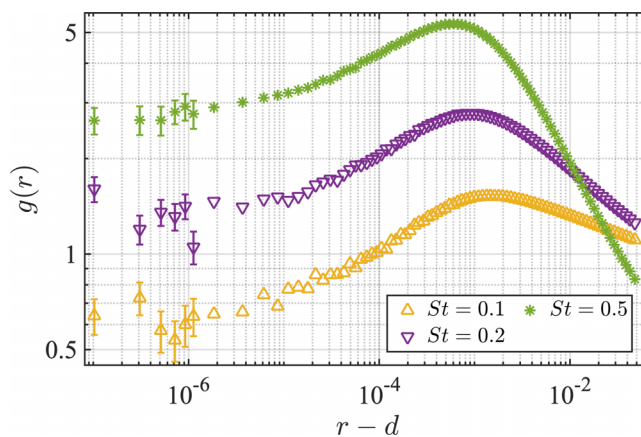


FIG. 4. High resolution plots of RDFs versus $r - d$ for cases of $St = 0.1, 0.2$, and 0.5 , where the regime of smaller $r - d$ values is resolved more clearly. In order to compare them clearly, the RDF for $St = 0.5$ is translated down vertically to half of its original height. Error bars represent statistical error of one standard deviation. Within the range of uncertainty, the RDF no longer decreases after $r - d < 0.04d$ and levels off to a fixed value.

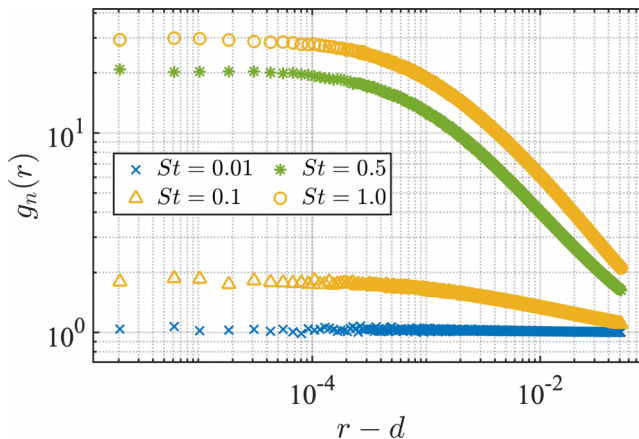


FIG. 5. The RDF for noncolliding particles (g_n) for different Stokes numbers. The particle diameter is $d = 9.49 \times 10^{-4}$ and $\text{Re}_\lambda = 124$. In log-log axes, g_n level off to plateau as the gap-distance $r - d$ approaches zero.

We end this section with a brief discussion of the significance of the above findings. As pointed out in Ref. [17], the fact that particle collision has effects on RDF suggests a significant implication that many results of earlier studies that assumed ghost particles should have limited relevance for prediction of actual particle collision rate. The previous statement is also true for particle systems that has any other collisional outcomes, e.g., hard sphere elastic collisions, but the specific modification the the RDF would be different. Any theoretical treatment of the collision rate should take into account the strong coupling among RDF, relative particle velocities and collision rate, such as in the theory presented in Ref. [17].

B. Collisional modulation factor

To further characterize the depletion zone of the RDF due to particle collisions, following the work of Saw and Meng [17], we assume that the RDF can be factorized such that $g(r) = \gamma_c(r)g_n(r)$, where $g_n(r)$ is the RDF for noncolliding (ghost) particles under the same physical environment. It is well known that, for monodisperse particles, $g_n(r)$ is a power-law of r/η [9,22]. However, as shown in Fig. 5, when plotted against $r - d$, g_n levels off to a plateau as r decreases toward d as a result of finiteness of $g_n(d)$. The collision-induced modulation factor, denoted as γ_c , is defined as the ratio of $g(r)$ to $g_n(r)$. The extent to which γ_c deviates from 1 reflects the degree of impact that collision-coagulation has on RDF. As depicted in Fig. 3, as the separation distance r increases, θ_m decreases, thereby reducing the influence of collision and coagulation on RDF [17]. Furthermore, for large r , as explained above, the rectilinear trajectories assumption breaks down and particles may have arbitrary velocity directions [17]. Thus, at a scale where r is significantly larger than the particle diameter d , collision has little effect on RDF and the value of γ_c equals to 1.

γ_c is calculated in each case and shown in Fig. 6. Because the trend of γ_c in the small-scale $r \sim d$ is more important, we plot them versus $r - d$. As expected, at large r , γ_c universally converges to unity, signifying that collisional effect is only noticeable at $r \sim d$. In the $r \sim d$ regime, however, we see that as St increases from a minute value (i.e., 0.01), γ_c gradually decreases, with smaller r being more affected. The rate of this decrease (with respect to St) is initially very weak, consistent with the hypothesis in Ref. [17] that γ_c is independent of St in the limit of small St . The observed rate of decrease becomes pronounced as St increases from 0.1 to 0.5. Beyond $\text{St} = 0.5$, γ_c seems to stagnate again until it reverses the trend and starts to increase significantly when St is greater than 1.0.

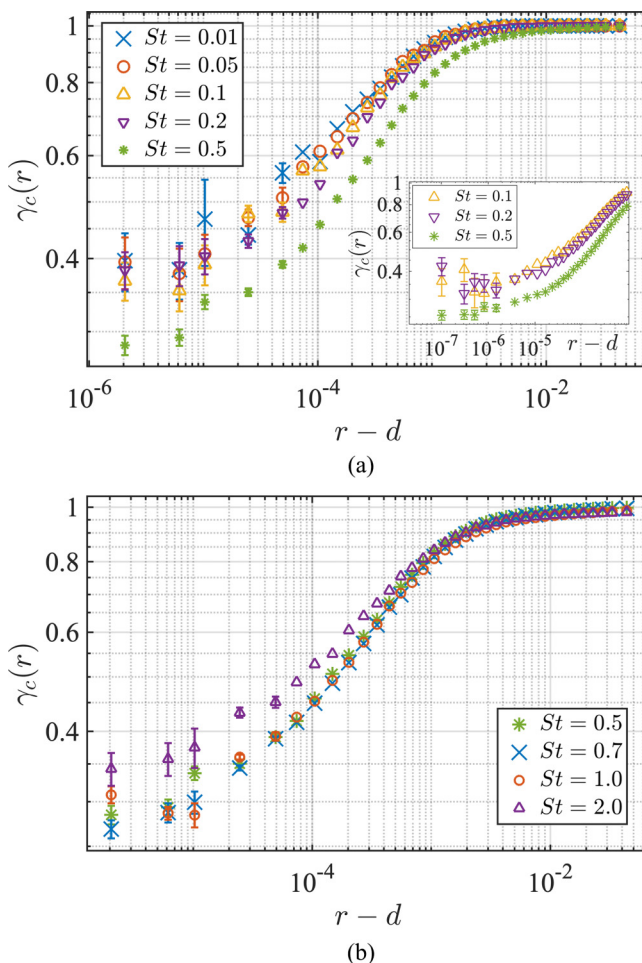


FIG. 6. The collisional modulation factor γ_c versus the gap-distance $r-d$ for particles with different Stokes numbers. The particle diameter is $d = 9.49 \times 10^{-4}$ and $\text{Re}_\lambda = 124$. Within the range of uncertainty, which is calculated as the standard error, γ_c is weakly dependent on St for $\text{St} \ll 1.0$ and it decreases as St increases from around 0.1 to 0.5.

This implies that when the Stokes number of the particles is much smaller than 1.0, the influence of the collision on the RDF is insensitive to the Stokes number. As the Stokes number increases, the influence of the collision increases and peaks at $\text{St} = 1.0$, which is similar to the trend of the power (c_1) of inertial clustering [22]. To see the trend of γ_c at small r more clearly, using the cases of $\text{St} = 0.1, 0.2$, and 0.5 as examples, we plot in the inset of Fig. 6(a), γ_c versus the gap distance $r-d$. Again, we see that γ_c follows a semi-power-law for $r-d$ in the range of $1 - 6 \times 10^{-4}$. For smaller $r-d$, the curves flatten and level off to a finite value.

For the sake of comparison, let us recall from earlier works [8,9,22] that g_n is a negative power law of r in the regime of $r/\eta \lesssim 20$, i.e., $g_n(r) = c_0(r/\eta)^{-c_1}$, where c_1 scales as St^2 for $\text{St} \ll 1$. We now attempt to derive an analogous relationship between γ_c and the Stokes number. From Fig. 6, γ_c seems to follow a quasi-power-law for gap distances ($r-d$) in the range $10^{-4} \lesssim r-d \lesssim 7 \times 10^{-4}$. We assume that in this range $\gamma_c = \tilde{c}_0(r-d)^{\tilde{c}_1}$. The relationship between \tilde{c}_1 and St is shown in Fig. 7. For $\text{St} \ll 1$, considering the level of statistical uncertainty, there is a weak tentative trend of increasing \tilde{c}_1 with Stokes number.

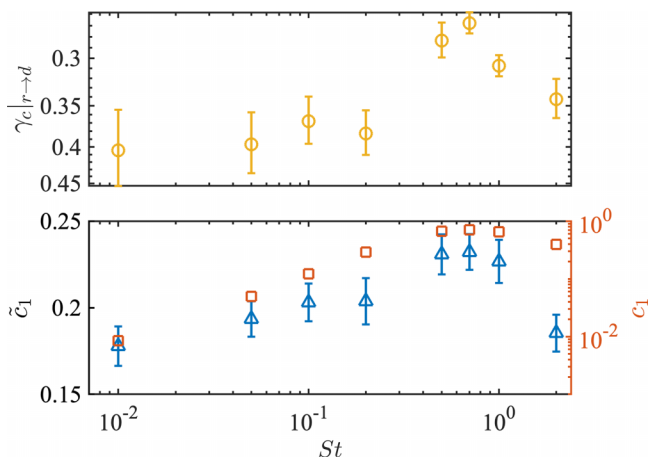


FIG. 7. Top: the value of γ_c at $r \rightarrow d$ ($r - d \sim 0.02d$) is shown as yellow \circ and its error bars represent one standard error. Bottom: the value of exponent of the power-law \tilde{c}_1 in $\gamma_c = \tilde{c}_0(r - d)^{\tilde{c}_1}$ in the range $1 \times 10^{-4} \lesssim r - d \lesssim 7 \times 10^{-4}$, which is shown as blue \triangle and based on the left vertical axis. The horizontal and vertical axes are logarithmic. Error bars represent one standard error. The value of the exponent of the power-law c_1 , as defined in $g_n = c_0(r/\eta)^{-c_1}$, obtained from DNS results in the range $0.1 \lesssim r/\eta \lesssim 1$, is shown as red \square and based on the right vertical axis. The statistical uncertainty of c_1 is smaller than the size of markers, therefore it is not shown in this figure. The vertical and horizontal axes in both top and bottom graph are logarithmic.

For comparison, we also show $c_1(\text{St})$ and $\gamma_c(r \rightarrow d)$ in Fig. 7, where $\gamma_c(r \rightarrow d)$ is the limiting value of γ_c at particle contact ($r = d$). The latter is of interest because it is closely related to the collision rate (in practice, we use the value of γ_c at $r - d \sim 2 \times 10^{-6}$ as this limit). It is important to note that the degree of variation of \tilde{c}_1 and $\gamma_c(r \rightarrow d)$ with St is much smaller than the degree of c_1 , especially for $\text{St} \ll 1.0$, the relationship with St is weak. Thus, for a first order theory, \tilde{c}_1 may be taken as a constant with respect to St given that the variation is as most 20%.

The above results indicate that for $\text{St} \ll 1.0$, the decrease in RDF caused by particle collision-coagulation is roughly independent of the Stokes number. While for large St (> 0.2), significant St -dependence is observed. Furthermore, the relationship between the decrease in RDF and St shows an observable, albeit weak, resemblance to that between the preferential concentration of particles and St . This implies that the Stokes number dependence of the RDF could not be completely decoupled from γ_c and that this issue merits further investigation.

In view of the significant Stokes number dependence of γ_c , we also conducted a complementary investigation on the Stokes number trend of the full RDFs [i.e., $g(r)$] as a comparative study. The RDFs for different Stokes numbers are vertically translated to overlap with the $g(r)$ for $\text{St} = 0.05$ at $r - d \sim 2 \times 10^{-4}$ to compare their shape. To show the influence on St more clearly, the RDFs for $\text{St} = 0.05$ and 0.7 are shown in Fig. 8 and the RDFs for $\text{St} \ll 1$ are shown in the inset. It can be seen that the slope of the RDF is almost constant for $\text{St} \ll 1$, but changes when considering larger St .

To summarize, for $\text{St} \ll 1$, the RDFs in the depletion zone exhibit near-universality, and the value of γ_c at $r \rightarrow d$ and its slope exhibit weak dependence on St . While for larger St , significant changes in both RDF and γ_c are observed. Previous research [10] has demonstrated that when $\text{St} \ll 1$, preferential sampling is the primary effect on particles and this sampling effect is dependent on Stokes number. As St increases, the path-history effect becomes increasingly important. This results in particles approaching each other at high relative velocities, a phenomenon known as “caustics” [23]. Thus it is expected that the Stokes number dependence become stronger in this regime. The findings of this study are generally consistent with this analysis.

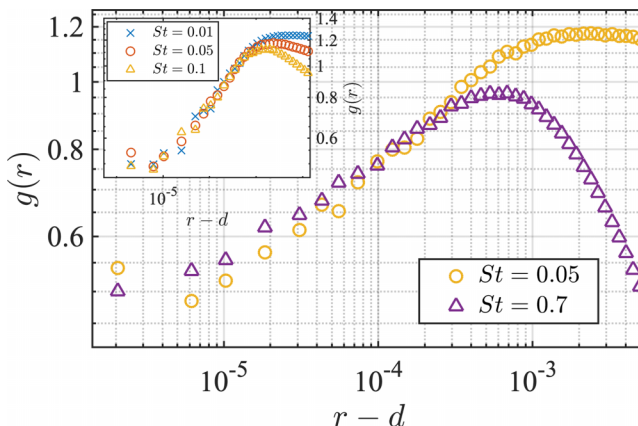


FIG. 8. The RDF for $St = 0.7$ is translated vertically down to 6.5% of its original height to compare the slope with $St = 0.05$. The translated RDFs for $St = 0.01, 0.05,$ and 0.1 are in the inset. The slope is the same for $St \ll 1$ but it is different for $St = 0.7$ and 0.05 . The position where the peak of RDF is related to St .

C. Reynolds number dependence

Statistics of Run 3, Run 11, and Run 12, listed in Table II, are used to investigate the influence of the Taylor-scaled Reynolds number Re_λ on the RDF. The RDFs for different Re_λ but the same St are shown in Fig. 9. The Stokes number is 0.1 and the parameters for three simulations are given in Table I. We see that in the range of small r , the RDFs of all cases overlap but for larger r , the RDFs are separated. However, when r is normalized by the Kolmogorov length scale η , as shown in the inset of Fig. 9, the RDFs now overlap at large r but are separated in $r \sim d$. It indicates that the position where the RDF decreases corresponding to r is related to particle diameter rather than to η . These results suggest that in the range of $Re_\lambda = 84$ –189, the statistics in the depletion zone, which are related to particle collision, are not affected by Re_λ , while the power regime related to the classical inertial clustering depends on Re_λ , but only through the change in Kolmogorov length-scale η .

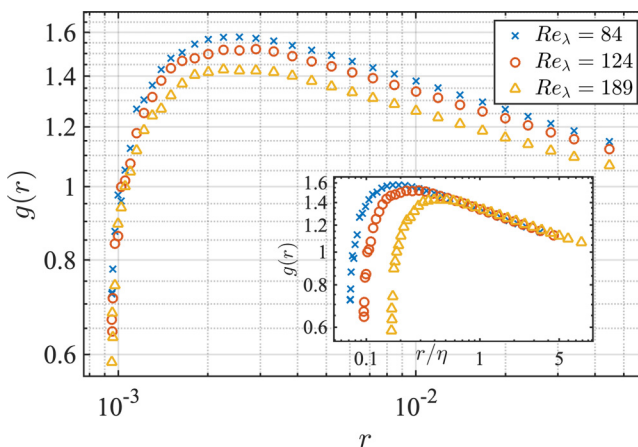


FIG. 9. The RDFs for particles in three cases with different Re_λ . The particle Stokes number is 0.1 and the diameter of particle is $d = 9.49 \times 10^{-4}$. (Inset) The RDFs as the function of r normalized by the Kolmogorov length η . The observed overlaps implies that Reynolds number effect is very weak.

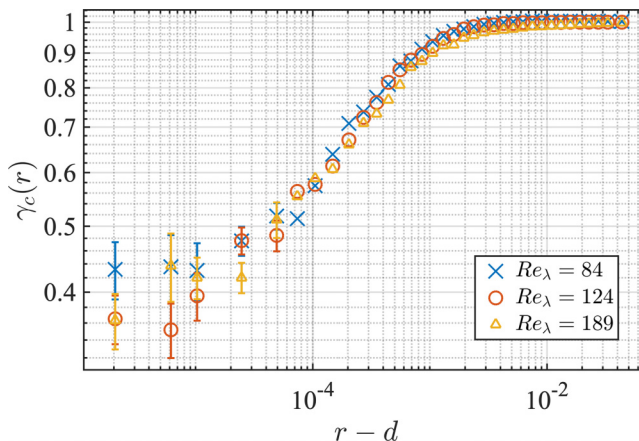


FIG. 10. The modulation factor γ_c versus $r - d$ for particles in three cases with different Re_λ . The Stokes number is 0.1 and the particle diameter $d = 9.49 \times 10^{-4}$. γ_c for three cases are overlapped within a range of uncertainty. Error bars represents standard deviation.

The modulation factor γ_c for these cases are shown in Fig. 10. We find that they overlap within the statistical uncertainty. This again suggests that the main characteristics of the depletion zone are insensitive to the flow Reynolds number from $Re_\lambda = 84$ to 189.

According to the Kolmogorov 1941 hypothesis [24], if the Reynolds number is large enough, then the statistics of the small scale of turbulent flow will not be influenced by of the large scale. Collisions occur on a scale of particle diameter, which here is much smaller than the Kolmogorov length scale, therefore, the decrease of RDF is insensitive to Re_λ . This view is consistent with the above results. However, in view of possible influence of sub-Kolmogorov scale intermittency [25,26], we acknowledge the fact that the range of Reynolds numbers investigated here is rather limited and future works involving higher Re_λ and spatial resolution may be necessary to address this question conclusively.

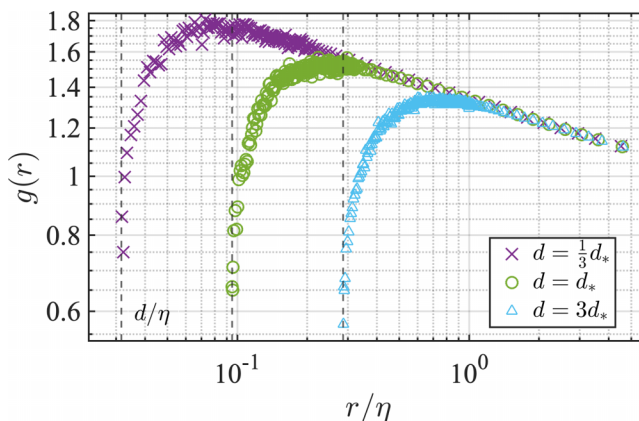


FIG. 11. The RDFs for particles with different diameters, $d = \frac{1}{3}d_*$, $d = d_*$, and $d = 3d_*$, respectively, in which $d_* = 9.49 \times 10^{-4}$. The Stokes number of particles is 0.1 and the Reynolds number of the flow is $Re_\lambda = 124$. The position where the RDF decreases closely follows to the particle diameter.

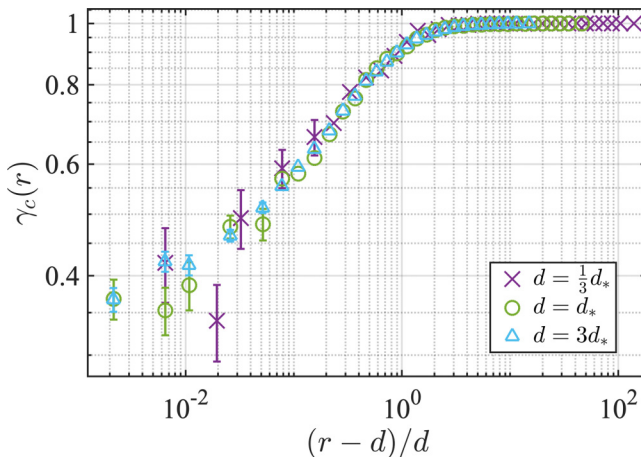


FIG. 12. The collisional modulation factor γ_c for particles with different diameters, $d = \frac{1}{3}d_*$, $d = d_*$, and $d = 3d_*$, in which $d_* = 9.49 \times 10^{-4}$. The Stokes number of particles is 0.1 and the Reynolds number of turbulent flow is $\text{Re}_\lambda = 124$. γ_c for all three cases coincide substantially.

D. Particle diameter dependence

The RDFs for particles of different diameters are shown in Fig. 11, the statistics used are from Run 3, Run 9, and Run 10. What is striking in Fig. 11 is that the position where the RDF starts to decrease is consistent with the particle diameter.

Since the particle diameters are different in the three cases, γ_c as a function of the rescaled gap distance $(r-d)/d$ is plotted in Fig. 12 to determine the relationship between the depletion zone of γ_c with the particle diameter. In this case, the modulation factors γ_c are coincidental, highlighting the central role of d .

The collision process of particles is strongly related to the particle size. Since we only consider the RDFs of monodisperse particles, we expected that the position where depletion zone begins is close to the particle diameter. The results shown here are in consistent with our expectations.

IV. DISCUSSION

The degree to which γ_c deviates from 1 represents the extent of the effect of collision on RDF. As illustrated in Fig. 6, the value of r corresponding to the point at which γ_c begins to decrease is almost the same for $\text{St} \ll 1$ but differs for larger values of St . As explained earlier (Fig. 3), when the particle separation distance r approaches the particle diameter d , the relative trajectory of the particle can be considered almost rectilinear. The larger the particle inertia (i.e., St), the longer it takes for the particle to change its original velocity and the greater the distance it travels during this time, implying the rectilinear assumption holds up to larger length scale. This increases the range over which collision and coagulation affect RDF. If we take r_{pc} as the separation distance r corresponding to the point at which γ_c begins to deviate from 1, then the value of r_{pc} should be related to the particle Stokes number, diameter, and potentially turbulent parameters; this will be a subject for future studies.

In Appendix B, we conclude that unresolved sub-Kolmogorov intermittency may slightly modify the inertial clustering exponent by a few percent. This shifts all small-scale features of the RDF upward by the same order of magnitude. As a result, the value of the RDF in this paper may be underestimated by a few percent. However, this effect on the trend of the RDF curve is minimal and does not impact significantly on the main results in this paper.

Previous research [26] indicates that the small-scale intermittency increases with Reynolds number. The range of Reynolds numbers investigated here is rather limited and may have a statistical

error of a few percent at most. Hence, future works with higher Reynolds numbers and spatial resolution may be necessary to conclusively address this question.

V. CONCLUSION

This paper studies the change in the radial distribution function (RDF) of particles subjected to the collision and coagulation (coalescence) interaction. We investigate the relationship between the RDF and the particle Stokes number, particle diameter, and Reynolds number. We find that the RDF decreases significantly at small particle separation distances r . When viewed as a function of $r - d$, we found evidence that the RDF does not decrease indefinitely, but levels off to a fixed value in the limit of $r \rightarrow d$. To study the relationship between the degree of reduction of the RDF and the particle and turbulent parameters, we separate the RDF into two multiplicative parts i.e., $g = \gamma_c g_n$, where g_n is the RDF for noncolliding particles under equivalent environment and γ_c is a collisional modulation factor that reflects the effect of particle collision on particle preferential concentration. We see that $g_n(r - d)$ levels off to a plateau as the argument $r - d$ approaches zero. However, the collisional factor γ_c universally converges to unity at large r and levels off to a fixed value at $r \approx d$. We find that γ_c depends on the Stokes number. Specifically, assuming a power-law model for γ_c in the range $0.1d \lesssim r - d \lesssim 0.7d$ [i.e., $\gamma_c = \tilde{c}_0(r - d)^{\tilde{c}_1}$], we find that in the small Stokes number limit, the value of \tilde{c}_1 is only very weakly dependent on St , while the overall Stokes number trend of \tilde{c}_1 is qualitatively similar to the power law exponent c_1 in the RDF of noncolliding (ghost) particles [i.e., $g_n(r)$]. It should be noted, however, that the increase in \tilde{c}_1 is much weaker than that of c_1 . The magnitude of γ_c at the limit $r \rightarrow d$ varies with the Stokes number following a trend similar to that of $\tilde{c}_1(St)$.

The preceding findings motivate a comparative investigation into the St trend of the full RDF, which has the result that the slope of the RDF $g(r)$ in the depletion zone is the same for $St \ll 1$ but it is different for large Stokes number (i.e., $St \geq 0.05$). Besides this, the location of the peak of RDF is found to be significantly St -dependent. These findings imply that the Stokes number dependence of the RDF could not be completely decoupled from γ_c [nor from $g(r)$] except in the regime of $St \ll 1$ where St dependence is weak.

We find that the shape of the RDF in the depletion zone ($r \sim d$) does not change with the variation of the flow Reynolds number within the range studied, i.e., $Re_\lambda = 84\text{--}189$ and the collisional modulation factor γ_c from different Re_λ overlap. However, further investigations involving larger Re_λ and higher spatial resolution may be needed to form stronger conclusion in this respect.

On the effect of particle diameter d , we find that larger d leads to the falling edge in γ_c occurring at larger values of $r - d$ (and r) such that the results coincide when γ_c is plotted against $(r - d)/d$.

All in all, for particles with $St \ll 1$, their RDFs in the depletion zone are almost universal for different St . And the collision scale, where the RDF and γ_c start to decrease, is only related to the particle diameter and is almost independent with St and Re_λ .

ACKNOWLEDGMENTS

This work was mainly supported by the National Natural Science Foundation of China (Grant No. 11872382) and by the Thousand Young Talents Program of China. E.W.S. also acknowledges that during his visit at the KITP, this work was supported in part by the National Science Foundation under Grant No. NSF PHY-1748958.

APPENDIX A: THE ENERGY SPECTRUM

The energy spectrum for three different turbulent flow in this paper are shown in Fig. 13. The detailed DNS parameters are give in Table I. It can be seen that the dissipation scale is well resolved.

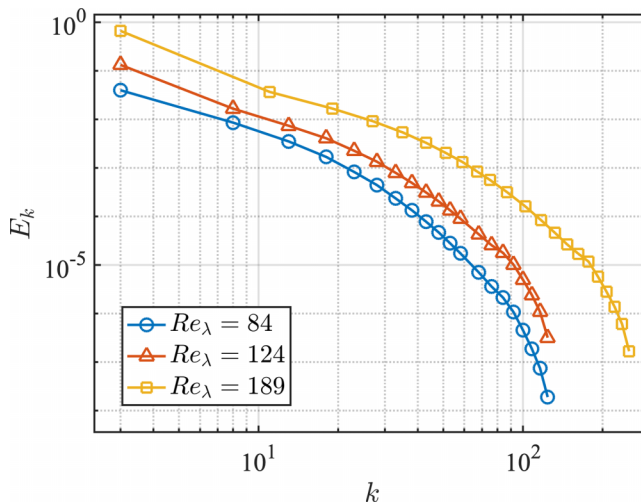


FIG. 13. The energy spectrum for different turbulent flow. $Re_\lambda = 84, 124,$ and 189 .

APPENDIX B: THE INFLUENCE OF THE SMALL-SCALE INTERMITTENCY ON THE RDF

In order to identify the effects of any sub-Kolmogorov scale flow features that may be present but under-resolved by the simulations at $N = 256$, an additional simulation at higher resolution (four times higher, i.e., at $N = 1024$) is conducted. The result and the corresponding comparisons are shown below.

For a discussion on sub-Kolmogorov intermittency, it is helpful to refer to the recent work of Buaria *et al.* [26]. They used DNS to investigate the sub-Kolmogorov-scale intermittency in turbulent flows at different Re_λ and found that the smallest scale at which sub-Kolmogorov intermittent features is observable scales inversely with the Reynolds number. One of the flows they studied which is most relevant to us is the one at $Re_\lambda = 140$, which they simulated using resolution of $N = 1024$. Their results and findings strongly suggest that such a flow should be well resolved at $N = 1024$. Thus, we follow this practice for our enhanced-resolution simulation mentioned above. However, a closer inspection reveals that our resolution is slightly below theirs in terms of $k_{\max}\eta$ (due to the different de-aliasing scheme employed). As a result, we contend that while our $N = 1024$ simulation may not capture, fully, the effects of sub-Kolmogorov intermittency, but should have at least captured most of the effects.

Table III presents the specific DNS parameters for both the original and additional simulations, while Figs. 14 and 15 compare the energy spectrum and the particles RDF, respectively. These spectra results indicate that the sub-Kolmogorov scale is better resolved at $N = 1024$. However, we must point out that the two flows are not exactly the same and fluctuate differently in time.

TABLE III. The DNS parameters and time-averaged statistics. N is the simulation grid size, ν is the kinematic viscosity of turbulence, ϵ is the dissipation rate of turbulent flow, u' is the root-mean-square velocity of turbulent flow, λ is the Taylor length scale, η and τ_η are the Kolmogorov length and timescale, L and T_L are the integral length and timescale, Re_λ is the Taylor scaled Reynolds number, and T_s is the length of time over which particle statistics are accumulated.

	ν	ϵ	u'	λ	η	τ_η	L	T_L	Re_λ	St	T_s
$N = 1024$	0.001	0.1011	0.5668	0.2183	0.0100	0.0994	0.6468	1.1411	123.7	0.1006	7.5 ($75.4\tau_\eta$)

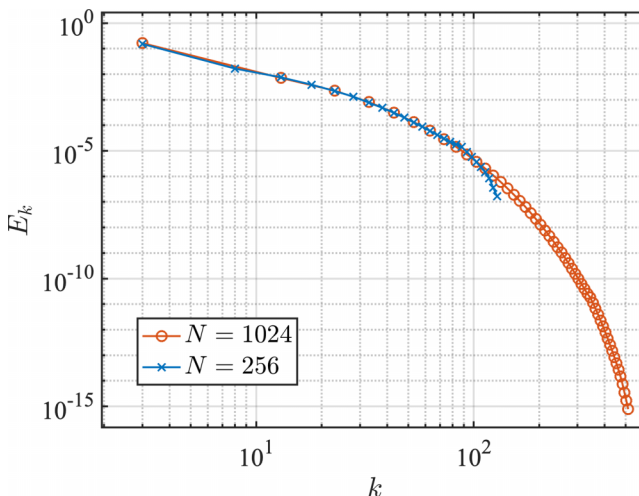


FIG. 14. The comparison of the energy spectrum under different simulations. The DNS parameters are listed in Table I flow 1 and Table III, respectively.

From the RDF comparison, we see that the two curves (both for $St = 0.1$) are very similar, but the RDF obtained at $N = 1024$ is slightly above the one at 256. Specifically, in the super-Kolmogorov inertial clustering regime, the power-law exponent c_1 is slightly altered such that the discrepancy in the magnitude of the two RDFs is at maximum about 2.5% (the 1024 case being higher), while at the collisional scale (the smallest scales), the difference is subject to statistical noise but on average is about 2.6% (the 1024 case being higher). From these, we conclude that the effect of unresolved sub-Kolmogorov intermittency may modify slightly (at most a few percents) the inertial clustering exponent. This in turn, would shift all small-scale features of the RDF upwards, by the same order of magnitude, but would not cause any significant changes to the qualitative trends observed in this paper.

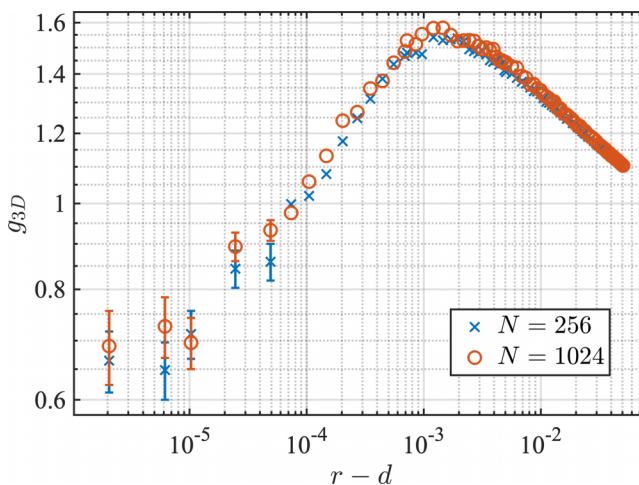


FIG. 15. The RDFs versus $r - d$ under different simulations. The DNS parameters are listed in Table I flow 1 and Table III, respectively.

- [1] R. A. Shaw, Particle-turbulence interactions in atmospheric clouds, *Annu. Rev. Fluid Mech.* **35**, 183 (2003).
- [2] W. W. Grabowski and L.-P. Wang, Growth of cloud droplets in a turbulent environment, *Annu. Rev. Fluid Mech.* **45**, 293 (2013).
- [3] J. N. Cuzzi, R. C. Hogan, J. M. Paque, and A. R. Dobrovolskis, Size-selective concentration of chondrules and other small particles in protoplanetary nebula turbulence, *Astrophys. J.* **546**, 496 (2001).
- [4] A. Johansen, J. S. Oishi, M.-M. M. Low, H. Klahr, T. Henning, and A. Youdin, Rapid planetesimal formation in turbulent circumstellar disks, *Nature (London)* **448**, 1022 (2007).
- [5] L. Pan, P. Padoan, J. Scalo, A. G. Kritsuk, and M. L. Norman, Turbulent clustering of protoplanetary dust and planetesimal formation, *Astrophys. J.* **740**, 6 (2011).
- [6] N. Smith, G. Nathan, D. Zhang, and D. Nobes, The significance of particle clustering in pulverized coal flames, *Proc. Combust. Inst.* **29**, 797 (2002).
- [7] K. D. Squires and J. K. Eaton, Preferential concentration of particles by turbulence, *Phys. Fluids* **3**, 1169 (1991).
- [8] W. C. Reade and L. R. Collins, Effect of preferential concentration on turbulent collision rates, *Phys. Fluids* **12**, 2530 (2000).
- [9] J. Chun, D. L. Koch, S. L. Rani, A. Ahluwalia, and L. R. Collins, Clustering of aerosol particles in isotropic turbulence, *J. Fluid Mech.* **536**, 219 (2005).
- [10] P. J. Ireland, A. D. Bragg, and L. R. Collins, The effect of Reynolds number on inertial particle dynamics in isotropic turbulence. Part 1. Simulations without gravitational effects, *J. Fluid Mech.* **796**, 617 (2016).
- [11] E. W. Saw, R. A. Shaw, S. Ayyalasomayajula, P. Y. Chuang, and A. Gylfason, Inertial Clustering of Particles in High-Reynolds-Number Turbulence, *Phys. Rev. Lett.* **100**, 214501 (2008).
- [12] J. P. Salazar, J. De Jong, L. Cao, S. H. Woodward, H. Meng, and L. R. Collins, Experimental and numerical investigation of inertial particle clustering in isotropic turbulence, *J. Fluid Mech.* **600**, 245 (2008).
- [13] P. Saffman and J. Turner, On the collision of drops in turbulent clouds, *J. Fluid Mech.* **1**, 16 (1956).
- [14] K. Gustavsson, B. Mehlig, and M. Wilkinson, Collisions of particles advected in random flows, *New J. Phys.* **10**, 075014 (2008).
- [15] S. Sundaram and L. R. Collins, Collision statistics in an isotropic particle-laden turbulent suspension. Part 1. Direct numerical simulations, *J. Fluid Mech.* **335**, 75 (1997).
- [16] L.-P. Wang, A. S. Wexler, and Y. Zhou, Statistical mechanical description and modelling of turbulent collision of inertial particles, *J. Fluid Mech.* **415**, 117 (2000).
- [17] E.-W. Saw and X. Meng, Intricate relations among particle collision, relative motion, and clustering in turbulent clouds: Computational observation and theory, *Atmos. Chem. Phys.* **22**, 3779 (2022).
- [18] R. S. Rogallo, *Numerical Experiments in Homogeneous Turbulence* (National Aeronautics and Space Administration, Washington, D.C., 1981), Vol. 81315.
- [19] V. Eswaran and S. B. Pope, An examination of forcing in direct numerical simulations of turbulence, *Comput. Fluids* **16**, 257 (1988).
- [20] M. R. Maxey and J. J. Riley, Equation of motion for a small rigid sphere in a nonuniform flow, *Phys. Fluids* **26**, 883 (1983).
- [21] P. J. Ireland, T. Vaithianathan, P. S. Sukheswalla, B. Ray, and L. R. Collins, Highly parallel particle-laden flow solver for turbulence research, *Comput. Fluids* **76**, 170 (2013).
- [22] E.-W. Saw, J. P. Salazar, L. R. Collins, and R. A. Shaw, Spatial clustering of polydisperse inertial particles in turbulence: I. Comparing simulation with theory, *New J. Phys.* **14**, 105030 (2012).
- [23] M. Wilkinson and B. Mehlig, Caustics in turbulent aerosols, *Europhys. Lett.* **71**, 186 (2005).
- [24] A. N. Kolmogorov, The local structure of turbulence in incompressible viscous fluid for very large Reynolds numbers, *Proc. Math. Phys. Eng.* **434**, 9 (1991).
- [25] J. Schumacher, Sub-kolmogorov-scale fluctuations in fluid turbulence, *Europhys. Lett.* **80**, 54001 (2007).
- [26] D. Buaria, A. Pumir, E. Bodenschatz, and P.-K. Yeung, Extreme velocity gradients in turbulent flows, *New J. Phys.* **21**, 043004 (2019).